This is a repository copy of *Application of electrochemical methods for studying steel corrosion in alkali-activated materials*.

White Rose Research Online URL for this paper:
https://eprints.whiterose.ac.uk/197033/

Version: Published Version

R E V I E W

Application of electrochemical methods for studying steel corrosion in alkali-activated materials

Shishir Mundra[1] | **Gabriel Samson[2]** | **Giulia Masi[3]** |
Rebecca Achenbach[4] | **David M. Bastidas[5]** | **Susan A. Bernal[6]** |
Maria C. Bignozzi[3] | **Maria Criado[7]** | **Martin Cyr[2]** | **Nina Gartner[8]** |
Stefanie von Greve-Dierfeld[9] | **Andraž Legat[8]** | **Ali Nikoonasab[10]** |
John L. Provis[11] | **Michael Raupach[4]** | **Gregor J. G. Gluth[10]**

[1]Institute for Building Materials (IfB), ETH Zurich, Zurich, Switzerland

[2]Laboratoire Matériaux et Durabilité des Constructions (LMDC), Université de Toulouse, Toulouse, France

[3]Department of Civil, Chemical, Environmental, and Materials Engineering (DICAM), Università di Bologna, Bologna, Italy

[4]Institute for Building Materials Research (ibac), RWTH Aachen University, Aachen, Germany

[5]National Center for Education and Research on Corrosion and Materials Performance (NCERCAMP-UA), Department of Chemical, Biomolecular, and Corrosion Engineering, The University of Akron, Akron, Ohio, USA

[6]School of Civil Engineering, The University of Leeds, Leeds, UK

[7]Eduardo Torroja Institute for Construction Sciences (IETcc-CSIC), Madrid, Spain

[8]Slovenian National Building and Civil Engineering Institute (ZAG), Ljubljana, Slovenia

[9]TFB Technology and Research for Concrete Structures, Wildegg, Switzerland

[10]Division 7.4 Technology Of Construction Materials, Bundesanstalt für Materialforschung und -prüfung (BAM), Berlin, Germany

[11]Department of Materials Science and Engineering, The University of Sheffield, Sheffield, UK

Correspondence

Shishir Mundra, Institute for Building Materials (IfB), ETH Zurich, CH-8093 Zurich, Switzerland.
Email: shishir.mundra@ifb.baug.ethz.ch

Gregor J. G. Gluth, Division 7.4 Technology of Construction Materials, Bundesanstalt für Materialforschung und -prüfung (BAM), 12205 Berlin, Germany.
Email: gregor.gluth@bam.de

Abstract

Alkali-activated materials (AAMs) are binders that can complement and partially substitute the current use of conventional cement. However, the present knowledge about how AAMs protect steel reinforcement in concrete elements is incomplete, and uncertainties exist regarding the application of electrochemical methods to investigate this issue. The present review by *EFC WP11-Task Force 'Corrosion of steel in alkali-activated materials'* demonstrates that important differences exist between AAMs and Portland cement, and between different classes of AAMs, which are mainly caused by differing pore solution compositions, and which affect the outcomes of electrochemical measurements. The high sulfide concentrations in blast furnace slag-based AAMs lead to distinct anodic polarisation curves, unusually low open circuit potentials, and low polarisation resistances, which might be incorrectly interpreted as indicating active corrosion of steel reinforcement. No systematic

study of the influence of the steel–concrete interface on the susceptibility of steel to corrosion in AAMs is available. Less common electrochemical methods present an opportunity for future progress in the field.

1 | INTRODUCTION

Corrosion of the embedded steel reinforcement is the primary cause of premature deterioration of reinforced concrete structures.[1] The direct and indirect costs associated with the corrosion in reinforced concrete structures can be as high as approx. 6% of the gross domestic product in industrialised countries, as in the case of the USA.[2] These enormous costs reflect three highly interrelated shortcomings in the areas of (1) our understanding of how corrosion takes place in real structures, which translates into (2) the reliability of standards used for monitoring corrosion in reinforced concrete structures and (3) our capability to accurately predict the service life of reinforced concrete structures. The last decades have seen significant advances in these three fundamental areas.[3–7] However, studies concerning steel corrosion in reinforced concrete structures, either in laboratory specimens or real structures, or representative pore solutions, have been focussed mainly on materials based on ordinary Portland cement (OPC) or OPC blended with supplementary cementitious materials (SCMs) such as blast furnace slag, fly ashes or calcined clays, simply because most of the concrete structures in the world have been made from these materials. Consequently, standards and recommendations on methods used to detect or qualify/quantify steel corrosion within a structure, generally apply only to conventional OPC-based materials.[8,9]

The push towards reducing emissions emanating from the cement industry has led to the development of several new binders mainly produced from waste streams or by-products of various industrial processes.[10,11] One set of such binders aimed at reducing emissions that have received immense academic and commercial interest are alkali-activated materials (AAMs). AAMs is a term used to describe a broad range of hardened binders that are produced by the reaction of an aluminosilicate precursor (such as blast furnace slag, coal fly ash, calcined clays and/or natural pozzolans) with an alkaline activator (alkali hydroxides, alkali silicates, alkali carbonates or sulfates).[11–13] Until very recently, the major focus of research on the durability of AAMs was the influence of aggressive species such as carbon dioxide and chloride on the chemistry of the binder, and the long-term durability of these materials has often been assessed based on the rate at which either the carbonation front progresses, or chloride penetrates from the external environment.[14–17] However, less attention has been directed toward the passivation and the depassivation of the steel reinforcement in these materials. The lack of reliable data relating to these issues may be one of the reasons for the slow uptake of these alternative binders in structural applications.

A major difficulty for the testing of reinforced materials based on alternative binders (including, but not limited to, AAMs) are unknowns regarding the applicability of electrochemical methods, testing protocols, and data interpretation and analyses used to assess the durability of these materials. Existing durability testing methods have been specifically tailored for application to the chemistry of OPC-based systems. The significant differences between the chemistry and the properties of AAMs and OPC have made the transfer and application of these methods in assessing the durability of reinforced AAMs difficult in most cases, and suggestions on how to mitigate the problems related specifically to the analytical methods and their evaluation have only recently begun to emerge. The present report, prepared by members of the *European Federation of Corrosion (EFC) Working Party 11-Task Force 'Corrosion of steel in alkali-activated materials'*, reviews the testing set-ups and electrochemical methods commonly used to assess corrosion initiation and propagation in steel-reinforced AAMs, and highlights peculiarities and difficulties in the interpretation of the results obtained in these specific cases. The report is not meant to be an introduction to the electrochemical methods, but rather to provide a guide on how to evaluate the resulting data specifically for AAMs and, thus, provide a starting point for further research and progress in this area.

2 | CURRENT STATE-OF-THE-ART IN ANALYSING STEEL CORROSION IN CONVENTIONAL CONCRETE

2.1 | General aspects of reinforcement corrosion and corrosion testing

Reinforcement corrosion in concrete structures is generally either due to the ingress of chloride ions and their subsequent build-up at the steel–concrete interface (SCI) above a 'threshold' concentration or due to a decrease of the pH of the concrete pore solution due to carbonation of the concrete cover[1] or due to leaching. Studies of the behaviour of steel reinforcement in cementitious materials have been performed either with the steel embedded in concrete or mortar or with the steel exposed to synthetic or expressed pore solutions of these materials.

The essential difference between the corrosion mechanisms and kinetics in concrete and mortars compared to solutions is the influence of a heterogenous porous medium in concretes and mortars on the transport of relevant compounds such as aggressive species, oxygen and, particularly, the buffering capacity of the solid phases[18–20] in the former. The relatively large dimensions of reinforced concrete elements, in some cases, cause a large distance between the anode and cathode, and consequently, the kinetics of the anodic and cathodic reactions can differ.[1,21,22] Anodic corrosion processes can occur very locally, damaging only a few square centimeters of the steel surface, while the large neighbouring steel surface remains passive. This indicates the separation of the anodic reaction and the cathodic reaction to form a macro-cell.[1,21,22] On the other hand, the distribution of anodic and cathodic sites on the micro-scale can also be very important.[7,23,24] Thus, general information on corrosion rate in concrete may be inaccurate if the corrosion mechanism is not clearly defined; it is important to know if corrosion takes place uniformly across the surface or occurs locally to be able to identify the most suitable mitigation strategies for extending the service life of a given structure. Commonly used electrochemical monitoring techniques generally do not enable a distinction between micro- and macro-cell corrosion. Therefore, in most cases, the corrosion damage can only be evaluated when the steel is destructively removed from the concrete.

Several methodologies and recommendations have been developed and employed to assess either the susceptibility of steel to corrosion or the severity of steel corrosion in concrete structures, many of them being developed and validated only for OPC-based binders. However, recent studies have highlighted the fact that the experimental data [critical chloride content (c_{crit}), carbonation depth (d_c), corrosion potential (E_{corr}), and corrosion current density (i_{corr})] commonly used to assess, describe and understand steel corrosion in concrete is scattered and requires further investigation, in particular, regarding the influence of different features at the SCI on the onset of corrosion.[4,7,23,25–27] Given the confounding nature of several variables that could influence the onset of corrosion in steel-reinforced concrete structures, it still remains rather unclear which characteristics of the SCI are the major determining factors.[7] This is further complicated by the fact that laboratory setups generally used to assess the susceptibility of steel corrosion in concrete differ from one laboratory to the other (Figure 1).
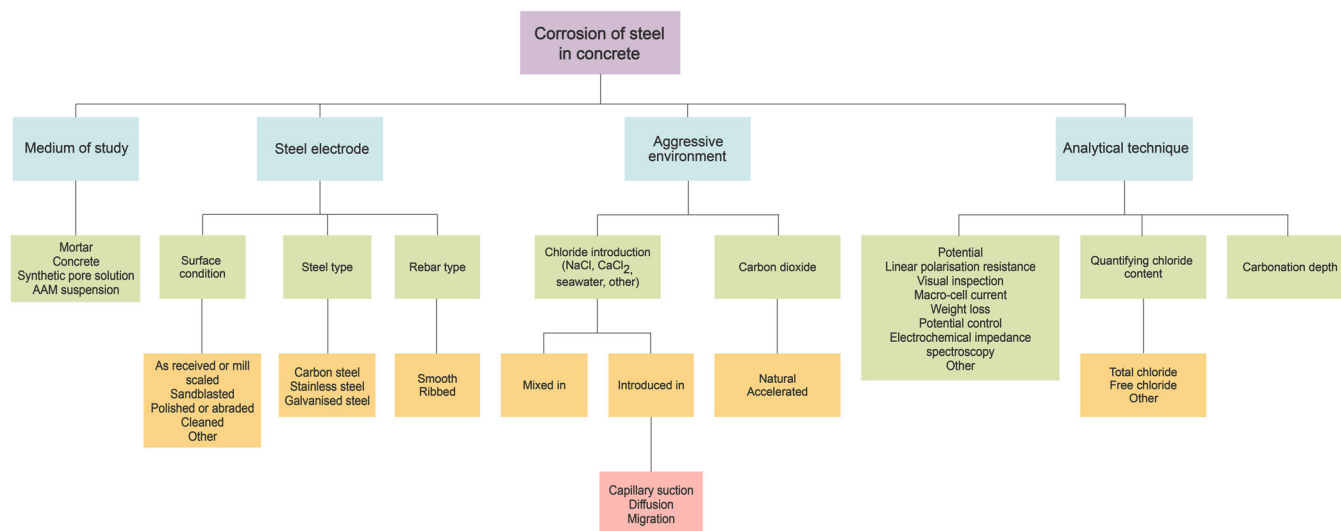

FIGURE 1 Flow chart showing some of the parameters that can be used to study the corrosion of steel in concrete at the laboratory scale. Adapted from Angst et al.[28]

2.2 | Standards and recommendations for conventional concrete

Most studies of the corrosion of steel in AAMs have referred to established standards and recommendations for OPC-based concretes to contextualise and classify their results. Therefore, a brief overview of the most important recommendations is given below, while no attempt is made to summarise the recent criticisms of these approaches with regard to conventional cementitious materials.

The ASTM C876-22b[29] is the most used standard for detecting corrosion in reinforced concrete. According to the standard, the probability of corrosion is determined according to the half-cell potential (The half-cell potential is often either referred to as the open circuit potential (OCP) or denoted by the symbol E_{corr}. The terms half-cell potential and OCP, and the symbol E_{corr} will be used interchangeably in this report) of the steel (Table 1), where the half-cell potential (vs. Cu/CuSO$_4$ sat.) is experimentally measured over the surface of a pre-wetted reinforced concrete element of interest (The half-cell potential is often either referred to as the open circuit potential (OCP) or denoted by the symbol E_{corr}. The terms half-cell potential and OCP, and the symbol E_{corr} will be used interchangeably in this report). Based on the guidelines specified in ASTM C876-22b,[29] areas where the embedded steel is expected to be active/passive are distinguished. It is noted that the values in Table 1 are mainly based on the investigations of 120 reinforced concrete bridge decks in the US exposed to chloride.[30,31] The measured half-cell potentials, based on the method prescribed by ASTM C876-22b,[29] do not allow the rate or extent of corrosion of the embedded steel reinforcement to be determined. The standard also advises caution when evaluating whether the steel is in the active/passive state in certain conditions or cases:

1. The carbonation depth has reached the surface of the embedded steel.
2. Indoor concrete elements that have not been subjected to frequent wetting, unless it has been protected from drying after casting.

3. Comparison of corrosion activity in reinforced concretes with highly variable moisture and oxygen content at the depth of the embedded steel.
4. Analysing corrosion activity in rehabilitated structures, where the moisture and oxygen content at the depth of the embedded steel may have been changed post-rehabilitation.
5. Conditions where oxygen concentration at the steel reinforcement is low, for example, for water-submerged structures.

The RILEM Technical Committee (TC) 154-EMC recommendation[8] focussed on the measurement of on-site parameters relevant to corrosion of the steel reinforcement embedded in concrete structures and the conclusions that could be drawn from various parameters. Based on published data and empirical analysis, several recommendations regarding the severity and probability of steel corrosion in concrete structures were developed.[8] In the case of measured half-cell potentials for steel embedded in concrete structures, recommendations on the interpretation of the data considered important parameters such as chloride contamination, carbonation, oxygen availability and the moisture content and degree of saturation (Table 2).

In addition, RILEM TC 154-EMC[9] proposed a classification of the severity of reinforcement corrosion based on nonuniform corrosion current densities for

TABLE 2 Typical ranges of E_{corr} (vs. Cu/CuSO$_4$) measured for carbon steel embedded in conventional concrete under different conditions.[8]

Condition	E_{corr}
Water saturated concrete without oxygen	$-0.90\,V > E_{corr} > -1.0\,V$
Wet, chloride contaminated concrete	$-0.40\,V > E_{corr} > -0.60\,V$
Humid, chloride free concrete	$+0.10\,V > E_{corr} > -0.20\,V$
Humid, carbonated concrete	$+0.10\,V > E_{corr} > -0.40\,V$
Dry, carbonated concrete	$+0.20\,V > E_{corr} > 0\,V$
Dry concrete	$+0.20\,V > E_{corr} > 0\,V$

TABLE 1 The probability of steel corrosion in conventional concrete classified according to measured E_{corr} (vs. Cu/CuSO$_{4sat}$), as specified in ASTM C876-22b.[29]

E_{corr}	Probability of corrosion
$E_{corr} > -0.20\,V$	10%
$-0.20\,V > E_{corr} > -0.35\,V$	Uncertain
$E_{corr} < -0.35\,V$	90%

TABLE 3 Ranges of nonuniform corrosion current density values (for localised corrosion) related to the significance in terms of service life of the reinforcement.[9]

i_{corr} (µA/cm^2)	Severity of corrosion
$\leqq 0.1$	Negligible
0.1–0.5	Low
0.5–1	Moderate
>1	High

localised corrosion calculated from measured polarisation resistances (using linear polarisation resistance (LPR) measurements; see Section 5.2) (Table 3), and recommendations regarding the interpretation of nonuniform corrosion current densities were given.

3 | MAIN DIFFERENCES BETWEEN AAMs AND CONVENTIONAL CEMENT

AAMs can be broadly classified, according to the bulk CaO content of the precursors, as low-Ca AAMs [molar CaO/(Si + Al) ratio ≈ 0] and high-Ca AAMs [molar CaO/(Si + Al) ratio ≈ 1].[13] Low-Ca AAMs such as alkali-activated fly ashes and metakaolin are characterised by a highly cross-linked alkali aluminosilicate (K-A-S-H/N-A-S-H) gel (Cement chemistry shorthand notation is used: $N = Na_2O$; $K = K_2O$; $C = CaO$; $A = Al_2O_3$; $S = SiO_2$; $H = H_2O$). Crystalline zeolites, such as faujasite-type, chabazite-type, gismondine-type and hydrosodalites, are commonly observed as secondary reaction products in low-Ca AAMs. The major reaction product in high-Ca AAMs such as alkali-activated blast furnace slags is an alkali- and aluminium-substituted calcium silicate hydrate (C-(N-)A-S-H) gel, possessing a disordered tobermorite-like structure. Depending on the MgO content in the precursor, hydrotalcite-like phases, AFm-group layered hydrous calcium aluminates and zeolites, such as gismondine and garronite, are often detected as secondary reaction products. Materials with Ca/(Si + Al) ratios between the limiting values shown above can also be produced, and usually show combinations of the binding phases listed here.

Since the reaction products of AAMs are significantly different from those encountered in OPC-based binders, their pore fluids also differ. The pore solution chemistry of AAMs is strongly dependent on the type of activator and aluminosilicate precursor. In the case of low-Ca AAMs, [Na+] and [OH−] were found to be between 0.60 and 1.60 M, and [Ca], [Si], and [Al] were close to 1 mM.[32,33] For high-Ca AAMs, in particular alkali-activated blast furnace slags, the concentration of soluble alkalis was also found to be higher than 1 M, and the concentrations of Ca, Al and Si generally between 0.01 and 10 mM.[32,34–36] Thus, the pore solutions of AAMs, in general, have higher concentrations of alkalis when compared to that of OPC, primarily due to the nature of the activator and the reaction mechanisms. With concentrations of counter-ion species such as aluminate and silicate being low, it can be inferred that the electro-neutrality of the pore solution is preserved by the presence of hydroxyl ions, therefore providing the pore solution with significant alkalinity to maintain the passivity of the reinforcement.[32]

TABLE 4 Examples of pore solution compositions of ordinary Portland cement (OPC) and CEM III/B,[39] a low-Ca alkali-activated material (AAM) (alkali-activated fly ash),[40] and a high-Ca AAM (alkali-activated blast furnace slag).[36]

Element/species/pH	OPC	CEM III/B	Low-Ca AAM	High-Ca AAM
Ca (mM)	1	0.2	0.7	0.4
Si (mM)	0.2	0.2	74	9.6
Al (mM)	0.1	0.1	0.3	4.3
Na (mM)	150	50	1443	1400
K (mM)	500	100	14	45
Total S (mM)	5	6	(391)[b]	550
S(−II) (mM)	n/a	n/a[a]	n/a	260
OH− (mM) [or pH]	600	150	628	[pH = 13.7]

Note: The pore solution compositions of the AAMs only serve as examples; they cannot be generalised for both low-Ca AAMs and high-Ca AAMs. The values for OPC and CEM III/B represent typical compositions.[39]

[a]Glasser et al.[41] determined [S(−II)] in the pore solution of a blend of 15% OPC and 85% blast furnace slag to be 3.7 mM.

[b]This value is possibly an outlier and not representative of low-Ca AAMs in general; cf. the full data set of Zuo et al.,[40] which includes pore solution compositions of low-Ca AAMs with considerably lower S concentrations.

One of the major differences between the pore solutions of low-Ca AAMs and high-Ca AAMs (alkali-activated blast furnace slags, in particular) arises due to the presence of reduced sulfur species (at concentrations as high as ~0.45 M[36,37]) in the pore solution of the latter. Blast furnace slag is a by-product of the iron-making process and retains the reducing nature of the furnace, containing approximately 1–3 wt.% sulfur. The reduced sulfur present in blast furnace slags readily dissolves and yields various aqueous sulfur species. In highly alkaline systems such as AAMs, the majority of the sulfur is expected to exist primarily as HS^- and/or S_n^{2-}, giving the alkali-activated blast furnace slags a reducing characteristic, while $S_2O_3^{2-}$, SO_3^{2-} and SO_4^{2-} may also be present.[36,38] Table 4 demonstrates the differences between the concentrations of various aqueous species in the pore solutions of OPC and CEM III/B (a blend of OPC and blast furnace slag), low-Ca AAMs (alkali-activated fly ash) and high-Ca AAMs (alkali-activated blast furnace slag).

4 | PARAMETERS INFLUENCING TEST RESULTS

4.1 | Reinforcement type and condition

For OPC-based binders, the type of steel used and the surface characteristics of the reinforcement both

influence passivation as well as depassivation behaviour,[7] and the same can be assumed to be the case for AAMs. Most of the studies concerning reinforcement corrosion behaviour in AAMs were conducted on conventional mild steel (in most cases ribbed rebars), and this will be the focus of this report. However, some studies have studied the corrosion of low-Ni steel,[42,43] stainless steel[42,44] and galvanised steel[45] in AAMs.

Several different surface conditions, such as as-received, sand-blasted, gently wire-brushed and degreased, have been used in the literature for analysing the corrosion of steel embedded in AAMs (Table 5). However, no systematic study exists highlighting the influence of various properties on the susceptibility to corrosion, when considering reinforced mortars/concretes made from AAMs. This is a serious and significant knowledge gap, given that it is well-known that the characteristics of the SCI strongly influence the corrosion behaviour and durability of reinforced concrete in the case of OPC-based binders.[7,23] This gap appears even more relevant if it is considered that, owing to the large variety of precursors, activators and mix designs applied to produce AAMs, the SCI in AAMs probably exhibits different and more varied features than the SCI in conventional concretes (as demonstrated by a study on the binder–aggregate interface in AAMs[72]). Only very few studies have focussed on the characteristics of the SCI in AAMs,[63,70] and it is therefore clear that this issue requires further research.

4.2 | Specimen geometry and setup

Many set-ups and sample geometries have been used for electrochemical measurements for the evaluation of steel corrosion behaviour in reinforced AAMs. Table 6 lists several of the methods applied for sample preparation and the electrochemical measurements carried out; some of the commonly applied electrochemical techniques will be discussed in more detail below (Section 5). Most of the studies reported results about the corrosion behaviour of steel rebars embedded in mortars, while only a few studies investigated the steel corrosion behaviour of reinforcements embedded in alkali-activated concretes. This is probably due to the higher complexity of producing and handling concrete samples, compared to mortars.

In most of the studies of steel corrosion in AAMs, only the central part of the steel reinforcement actively acted as a working electrode, while the external parts and the parts of the rebars close to the surface of the mortar or concrete specimen were isolated using adhesive tape, epoxy resin or acrylic tube, to avoid crevice corrosion

(Table 6). In one case, the steel reinforcement was welded with a stainless-steel wire,[63] leading to the preferential void formation at the SCI near the welding joint (likely during compaction of the mortar), which in turn led to preferential corrosion at these locations. Based on a round-robin test conducted by RILEM TC 235-CTC,[20] it has been proposed that if stable corrosion takes place within less than 14 days after the start of exposure to chlorides, whether due to the transport of aggressive species through cracks or heterogeneous features at the SCI, or due to crevice corrosion, the results may not be representative of real-world corrosion and should be discarded.[20] In any case, specimens showings signs of crevice corrosion must be removed from the subsequent analysis, as is a common standard.

The corrosion studies were generally conducted using a three-electrode setup, where the reference electrode [usually Ag/AgCl, saturated calomel electrodes (SCE), or Cu/CuSO$_4$] was either embedded in the specimens or immersed in a solution or placed on the concrete surface. The counter electrodes (usually stainless steel, titanium, graphite, or mixed metal oxide) were applied as an external mesh immersed in solution, and in some cases, embedded within the concrete or mortar.

Table 6 demonstrates that a wide variety of sample geometries, preconditioning, and testing arrangements were used for the evaluation of the corrosion of steel bars in AAMs. These significant differences between experimental setups are likely responsible for some of the differences between the outcomes of these studies, which makes it difficult to deduce details of the corrosion mechanisms of steel in these materials. However, some general conclusions can be drawn from the results, as will be discussed in the following sections.

In addition to the studies of reinforcement corrosion in AAM mortar and concrete specimens, a number of related studies have been conducted in synthetic pore solutions.[43,48,53,55–57,59,65,66] Though the conditions in these experiments differ from the conditions of reinforcement corrosion in concretes in several respects (e.g., absence of the SCI), some of these studies have led to important insights that help to explain observations for steel in AAMs, as will become apparent in the discussions below.

4.3 | Exposure to aggressive species

The highly alkaline nature of the pore solution of concrete generally allows the steel reinforcement to attain and remain in the passive state. For corrosion studies, reinforced specimens are usually exposed to an aggressive environment for different durations before

TABLE 5 Examples of steel type and steel surface conditions in studies of reinforcement corrosion in alkali-activated materials (AAMs) mortars and concretes and synthetic AAM pore solutions.

Steel grade	Rebar diameter[a]	Steel chemical composition[a]	Surface condition[a]	Reference
C-steel	6 mm	NR	NR	[46, 47]
AISI S32001; AISI 304; C-steel	10 mm	R	NR	[42]
C-steel	10 mm	R	NR	[48]
C-steel	10 mm	NR	NR	[49]
Low-Ni; AISI 304; C-steel	10 mm (NC)	R	As-received and degreased	[43]
C-steel (1018)	6 mm	R	Sand-blasted	[50]
Normal ductility C-steel with 500 MPa yield strength	12 mm	NR	Gently wire-brushed	[25]
C-steel	10 mm	R	NR	[51]
C-steel	NR	NR	Wire-brushed and dry cleaned	[52]
C-steel	10 mm (ribbed)	NR	Sandblasted and degreased	[53]
C-steel	10 mm (ribbed)	NR	Sandblasted	[54]
Mild C-steel (grade B500)	12 mm	R	Polished with SiC abrasive paper (240–600 grit) and degreased with acetone	[55, 56]
LC-steel and 00Cr10MoV (400 MPa)	NR	R	Polished with SiC abrasive paper (up to 1200 grit) and then with diamond polishing agent. Cleaned by ethanol	[57]
C-steel	20 mm	NR	NR	[58]
C-steel (hot rolled ribbed – HRB 400)	16 mm	R	Polished by SiC abrasive paper (up to 1200 grit) and by 3 mm monocrystalline diamond suspension. Then ultrasonically with alcohol for 5 min.	[59]
C-steel (500 MPa yield strength)	12 mm	NR	Gently wire-brushed	[60]
C-steel	12 mm	R	As-received	[61]
C-steel	12 mm (C)	R	As-received	[62]
C-steel (BSt 500)	10 mm (C)	NR	NR	[63, 64]
Hot rolled ribbed C-steel (20MnSiV)	NR	R	Polished by SiC abrasive paper (up to 1200 grit) and then with diamond polishing agent. Cleaned with ethanol	[65]
C-steel Galvanised steel	8 mm	NR	Galvanised steel rebars obtained by hot-dipping the bare steel rebars in a pure Zn bath at $T = 445°C$ for 5 min	[45]

(Continues)

TABLE 5 (Continued)

Steel grade	Rebar diameter[a]	Steel chemical composition[a]	Surface condition[a]	Reference
C-steel (Q235)	NR	R	Polished with sand papers (from 300 to 1500 grit) and polished with a flannelette	[66]
C-steel	10 mm	NR	NR	[67]
C-steel	6 mm	NR	NR	[68]
C-steel	6.4 mm	NR	Cleaned by acetone	[69]
C-steel ('conventional reinforcing steel')	16 mm	R	NR	[70]
C-steel ('cold rolled, B 500B reinforcing steel bar')	6 mm	NR	NR	[71]

[a] Abbreviations: C, corrugated; NC, not corrugated; NR, not reported; R, reported.

conducting electrochemical analysis of the steel responses to infer whether corrosion initiation has occurred or to determine the degree of corrosion of steel rebars. In reinforced AAMs, similar approaches to those applied to OPC-based materials are adopted to induce the transport of aggressive species into the samples to be tested, which are briefly described in this section.

Ponding tests (e.g., NT BUILD 443[74]) with either a solution simulating the Cl^- concentration of seawater (3.5% NaCl) or with a higher Cl^- concentration have been the most commonly used test setups to introduce chloride ions to initiate chloride-induced corrosion (Table 6). To avoid the leaching of alkali ions and/or Ca^{2+}, the exposure solution is often a mixed solution of NaCl and either NaOH or $Ca(OH)_2$. Depending on the cover depth, the type of cement, and the water/binder ratio (w/b) of the specimens, the time to achieve detectable levels of corrosion in this set-up can be very long, if no additional measures are adopted.

To accelerate Cl^- ingress and thereby achieve meaningful results in a laboratory setup faster than with only diffusion of Cl^-, the use of wetting/drying cycles has often been employed.[25,52,60,71] These cases are also nearly representative of concrete in a splash or tidal zone (exposure classes XD3 and XS3, respectively, according to EN 206[75]), which is known to be the most critical condition for steel-reinforced concrete.

Another way of accelerating Cl^- ingress through the concrete cover towards the steel reinforcement is through the application of an externally applied electrical field.[76,77] Under the influence of an applied potential difference between the anode (at the level of the steel reinforcement embedded in the concrete) and the cathode (on the surface of the concrete, immersed in a reservoir of a chloride-containing salt solution), Cl^- migrate from surface of the concrete towards the anode at the level of the steel reinforcement. The Cl^- threshold concentration is assumed to be reached at the moment when the steel reinforcement exhibits a sudden drop of the polarisation resistance, indicative of the onset of corrosion. A 10 V potential difference between the anode and the cathode has been recommended to drive the chloride ions from the reservoir solution (composed of 1 M NaCl solution) toward the anode for conventional concretes.[76,77] The two major challenges associated with this test setup are the polarisation of the steel reinforcement due to an externally applied electrical field resulting in incorrectly measured polarisation resistances, and the migration of other negatively charged anions such as OH^- towards the anode, which could lead to a change in the pH of the pore solution around the steel reinforcement and can also influence the migration of Cl^-. Moreover, the polarisation

TABLE 6 Examples of sample preparation, exposure conditions and performed electrochemical tests in studies of reinforcement corrosion in alkali-activated materials (AAMs) mortars and concretes.

Sample preparation	Exposure and performed tests[a]	References
Embedded in small prismatic samples ($8 \times 5.5 \times 2$ cm). Central active zone of 10 cm^2 to isolate the mortar/steel interface	Admixed CaCl$_2$: OPC, LPR, anodic polarisation, GPM	[46, 47]
Embedded in small prismatic samples ($8 \times 5.5 \times 2$ cm). Active surface area of 5.6 cm^2 marked with adhesive tape to isolate the mortar/steel interface	Accelerated carbonation, subsequent immersion NaCl solutions: OCP, LPR, EIS, anodic polarisation	[42]
10-mm height steel cylinders embedded in epoxy resin (exposed area of 0.78 cm^2) and ground with SiC papers up to grade 4000 and polished with 1 μm diamond paste; Bars embedded in mortar prisms	Carbonation and immersion in 1% NaCl solution: OCP, EIS	[48]
Embedded in prismatic samples ($28 \times 11.4 \times 15$ cm). The upper and lower bars (length = 381 mm) placed longitudinally 25 mm from the top and the bottom	Subjected to wet and dry saltwater cycles up to 364 days: OCP, LPR	[49]
Embedded in mortars. Active surface area of 10 cm^2 marked with adhesive tape to isolate the mortar/steel interface	650 days of partial immersion in NaCl solutions with increased salt concentration: OCP, EIS, anodic polarisation	[43]
Deformed rebar (length of 300 mm) embedded in the center of concrete cylinders	Accelerated carbonation: OCP, LPR, steel/concrete interface inspection	[50]
50-mm long bars machined at both the ends. An acrylic tube attached at each rebars end and sealed with silicone. Cu wire welded on each steel bar. Both top and bottom sides of the samples coated with anti-chloride resin to enforce peripheral Cl$^-$ penetration	Wet and dry test up to 11 months: OCP, LPR, ZIR, anodic/cathodic polarisation, gravimetric mass loss	[25]
100-mm long bars coated with different sol-gel coatings. Two bars embedded in prismatic samples ($8 \times 5.5 \times 2$ cm)	After carbonation, partial immersion in NaCl solution (3 wt%) up to 240 days: OCP, LPR, EIS	[51]
Four rebars embedded in prismatic samples ($25 \times 25 \times 11$ cm) together with stainless steel electrode (to measure the electrical resistivity of the concrete)	Wet and dry test up to 250 days: gravimetric mass loss	[52]
Two rebars embedded in prismatic samples ($20 \times 25 \times 5$ cm) with the ends masked with epoxy resin and isolated with thermo-shrinking adhesive tape to have an exposed area of 74 cm^2. Embedded in the sample, also two activated Ti wires (reference electrode) and three symmetrically arranged SS bars (counter electrode)	Partial immersion in 3.5% NaCl solution (monthly renewed) up to 90 days: OCP, LPR, EIS	[53]
Embedded in cylindrical samples (10×3.5 cm) along the longitudinal axis (mortar cover of 1.3 cm) with both the ends masked by epoxy resin. Epoxy resin applied also on the reinforced samples to expose only the surfaces corresponding to the exposed bar	Wet and dry cycles in 0.1 M NaCl solution (4 days of immersion and 3 days of dry) up to 100 days: OCP, LPR, anodic polarisation, EIS	[54]
Embedded in prismatic samples ($9.5 \times 9.5 \times 30$ cm)	After curing, partial immersion in 2.83 M and 0.6 M NaCl solutions up to 500 days: OCP, LPR	[58]
Embedded in prismatic samples ($13 \times 10 \times 10$ mm). 50-mm long bars machined at both the ends. An acrylic tube attached at each rebars end and sealed with silicone	Natural and accelerated carbonation: OCP, LPR	[73]
Embedded in cylindrical samples (5×10 cm), 50-mm long bars machined at both the ends. An acrylic tube attached at each rebars end and sealed with silicone	Partial immersion in 3.5% NaCl solution: OCP, LPR	[60]

(Continues)

TABLE 6 (Continued)

Sample preparation	Exposure and performed tests[a]	References
2 rebars embedded in each prismatic sample ($8 \times 5 \times 5$ cm). Ends masked with epoxy resin coating (exposed area of $10 \, cm^2$)	Immersion in 1 M NaOH solution and 1 M NaOH + 3.5% solution up to 150 days: OCP, EIS, anodic polarisation	[61]
Embedded in prismatic samples ($8 \times 5 \times 5$ cm) with the ends masked with epoxy resin coating (exposed area of $10 \, cm^2$)	Immersion in different NaOH and $Ca(OH)_2$ solutions with 3.5% NaCl up to 180 days: OCP, LPR, EIS	[62]
Corrugated rebars (length of 120 mm) embedded in prismatic mortar specimens. Stainless-steel wire welded	Leaching in deionised water and immersion in 1 M NaCl solution; accelerated carbonation: OCP, GPM	[63, 64]
Four rebars embedded in cylindrical concrete samples (concrete cover of 15 mm) with an exposed area of $16 \, mm^2$ (epoxy resin applied on the reinforcements)	12 weekly wet and dry cycles in a 3.5% NaCl solution: OCP, LPR (in dry and wet conditions)	[45]
Ribbed rebars (length of 120 mm) embedded in concrete cubes. Cu wired welded to each bar and sealed by epoxy resin	Immersion in 3% NaCl solution for 1 week, then 2 week-dry cycles: LPR	[67]
Embedded in mortar cylinders with a mortar cover of 7 mm. An insulating tape was applied to have an exposed area of $12.3 \, cm^2$	Different environments (humid chamber, accelerated carbonation, partial immersion in 3.5% NaCl solution, sample fabrication with different NaCl concentrations: OCP, LPR	[68]
Steel rod (with a length of 150 mm) embedded in concrete. An insulating tape was applied to have an exposed area of 50 mm in length	Accelerated carbonation process: LPR	[69]
Rebar (length: 200 mm) embedded in mortar. Epoxy coating applied at the ends, leaving an exposed area of $50.3 \, cm^2$. Copper wire welded	Immersion in 3.5% NaCl solution; natural carbonation in marine environment: OCP, EIS	[70]
One steel rod in prism-shaped mortar specimen ($3 \times 3 \times 10$ cm). Epoxy-based coating applied at the steel ends, leaving an exposed area of $17 \, cm^2$. 7 mm of mortar cover. Specimens cured in a humidity chamber for 28 days	Wet/dry cycles with 3.5% NaCl solution (17 cycles): EIS (once per cycle, wet conditions), μXCT scans (before and after exposure)	[71]

[a]Abbreviations: EIS, electrochemical impedance spectroscopy; GPM, galvanostatic pulse measurement; LPR, linear polarisation resistance; OCP, open circuit potential; μXCT, X-ray computed microtomography; ZIR, a method related to EIS for measuring ohmic drop.

of the steel reinforcement will lead to acidification of the pore solution at the SCI.[78]

Another approach is to introduce NaCl or $CaCl_2$ as an admixture in the concrete or mortar used to produce the reinforced AAM specimens.[42,46,47,67] However, accelerating chloride-induced corrosion using such a setup has major drawbacks and should be avoided according to current recommendations.[20] The distribution of Cl^- in the concrete is essentially homogeneous in this setup, which deviates from what is observed in real structures exposed to external Cl^-, and the presence of chlorides from early on can interfere with the formation of the passive layer as would be observed in real structures. In addition, depending on the binder type, the hydrated phase assemblage and, thus, the pore solution composition of the concrete at the SCI might be different from systems without the addition of chlorides.

Carbonation of the concrete cover through both natural carbonation (i.e., at the atmospheric CO_2 concentration of 0.04%) and accelerated carbonation (i.e., at higher than atmospheric CO_2 concentrations) has been applied to investigate the depassivation and the corrosion rate of steel in carbonated AAM concrete/mortar specimens (Table 6). As for chloride penetration, the use of accelerated methods to induce depassivation has the advantage of yielding results faster, but this approach may come with certain complexities or drawbacks. The carbonation of AAMs under customary accelerated conditions (i.e., CO_2 concentrations ≥ 1%) leads to the formation of other carbonation products and lower final pH values compared to what is observed under natural carbonation, and this may yield conditions at the SCI and behaviour of the steel reinforcement that are not representative of real-world conditions.[73,79] The effect of carbonation on steel corrosion in AAMs is not

well understood neither under natural nor under accelerated carbonation conditions. Consequently, there is an urgent need to elucidate how carbonation in these materials and the associated changes in the microstructure and pore solution composition influence the stability of passive films forming in steel embedded in these materials.

An additional issue that should be borne in mind when analysing the corrosion of steel in carbonated AAMs is that the corrosion rate is also strongly dependent on the moisture state at the SCI. Thus, while it is often assumed that steel corrosion commences once the carbonation front reaches the SCI, this is not necessarily the case. The importance of the moisture conditions at the SCI for steel corrosion in carbonated conventional concretes has been stressed in recent publications,[4,80,81] while studies in this regard for AAMs are not available.

5 | COMMONLY APPLIED ELECTROCHEMICAL TECHNIQUES

5.1 | OCP

The OCP, also referred to as the corrosion potential (E_{corr}), can be described as the potential difference between a reference electrode and the working electrode in a particular electrolyte, when the cell is switched off and no external current/voltage is applied. In concrete specimens, the OCP of the steel reinforcement can be measured according to the method specified in ASTM C876-22b[29] or the recommendations of RILEM TC 154-EMC.[8] The OCP of a particular system conveys important information and can, in principle, be used to assess whether corrosion occurs or not through application of Pourbaix diagrams.[82] However, while the OCP can yield information on the probability of finding corroding locations within a concrete structure, it cannot inform the user of the kinetics or the degree of corrosion. Moreover, as discussed by Elsener et al.,[8] a low potential does not necessarily indicate active corrosion of the steel reinforcement, as a low potential can be caused by various factors such as oxygen availability, the resistivity of the concrete, use of SCMs, and degree of saturation of the concrete. Therefore, to unambiguously detect the onset of steel corrosion in laboratory experiments, a clear drop in the potential, on transitioning from the passive to the active state, needs to be observed. A shift in the corrosion potential of the embedded steel reinforcement by approximately −200 mV has been established as a criterion indicating the transition from the passive to the active state for conventional concretes,[83,84] and subsequently adopted for AAMs.[63] Since both passivation and depassivation of the steel reinforcement are time-dependent phenomena, it is essential that sufficient time is allowed for the steel reinforcement to reach a steady passive or active state before the OCP is recorded.

The OCP measured for steel in the passive state in mortars/concretes made of low-Ca AAMs, tends to be similar to those observed in OPC-based materials[46,47,63] or slightly lower.[25,42,53] The lower OCP in the latter studies could be related to either a lower pH in the mortars/concrete specimens in those studies or a lower oxygen availability at the SCI due to the degree of saturation in the test setups.[25] These observations are in line with the finding that the mechanisms of passivation and the composition of the passive film formed on steel in synthetic pore solutions simulating low-Ca AAMs are similar to that observed for steel in OPC, with the inner layer being a dense Fe (II, III) oxide, surrounded by an outer layer of a hydrated Fe (III) oxide/hydroxide.[55] However, the establishment of a stable passive film on reinforcing steel in low-Ca AAMs may require several weeks,[45,85] that is, considerably more time than in OPC-based materials, and this must be considered in studies of steel depassivation and corrosion onset in AAMs (which usually assume the steel to be in the passive state at the beginning of exposure).

The OCP values of steel in alkali-activated blast furnace slags (high-Ca AAMs) have been observed to be much lower than those observed in OPC as well as low-Ca AAMs, viz., in the range −400 to −700 mV versus Ag/AgCl.[61,62,86] Correspondingly, Angus and Glasser[87] deduced that sulfides from blast furnace slag in blended slag-Portland cement can lower the OCP of steel in these materials to between −250 and −400 mV versus SCE, and other researchers[88,89] found OCPs in the range approx. −300 to −700 mV versus SCE for blast furnace slag-containing cement. Recent work on steel exposed to alkaline solutions with varying concentrations of sulfide[56] has explained these observations with the consumption of oxygen by reduced sulfur species (released from the blast furnace slag in the aforementioned cement and AAMs), leading to reducing (oxygen-depleted) conditions in the electrolyte solution surrounding the steel. This was deduced from the results of a variety of analytical techniques, including cyclic voltammetry and anodic polarisation (cf. Section 5.4). An additional possible factor for the low OCPs is the lower porosity of alkali-activated slags compared to low-Ca AAMs, which could lead to lower availability of oxygen at the SCI.[61] As shown by X-ray photoelectron spectroscopy, an important consequence of the presence of significant concentrations of sulfide in alkali-activated blast furnace slags is that the surface layer of the steel is composed mainly of Fe-S complexes,[56] in
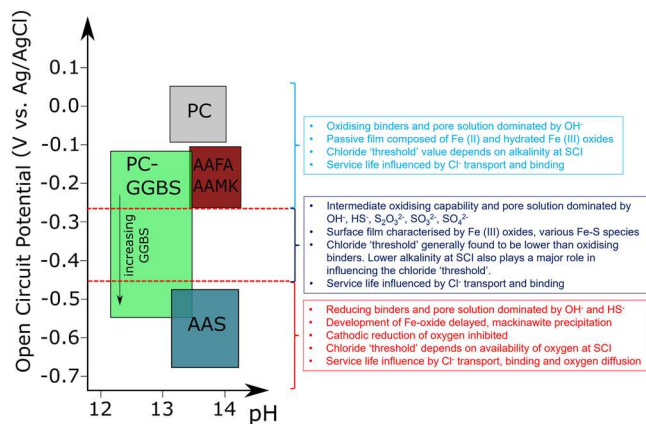
FIGURE 2 Overview of the conditions at the steel–concrete interface (SCI) of steel in cement and alkali-activated materials (AAMs) based on internal redox conditions before chloride ingress. AAFA, alkali-activated fly ashes; AAMK, alkali-activated metakaolin; AAS, alkali-activated (blast furnace) slags; GGBS, ground granulated blast furnace slag; PC, Portland cement; SCI, steel–concrete interface. (Reproduced from Mundra et al.[85] published under a Creative Commons license: https://creativecommons.org/licenses/by/4.0/ [CC BY 4.0]; a reference has been removed from the text).

contrast to the Fe oxide/hydroxide layers that form in OPC-based materials and low-Ca AAMs.

Based on the above findings, Mundra et al.[85] have developed a classification of the conditions at the SCI in different classes of binders, including AAMs, and how these affect the susceptibility of steel in these materials to chloride-induced corrosion initiation (Figure 2). The lower potentials typically found in high-Ca AAMs compared to OPC-based binders would yield misleading interpretations if the classifications proposed for the probability of corrosion by ASTM C876-22b[29] or the recommendations by RILEM TC 154-EMC,[8] developed for PC-based concretes (Section 2.2), are applied without modifications. Additionally, with such low OCP values, it might not always be possible to unequivocally observe a drop in the OCP of −200 mV to identify the transition of the steel reinforcement from the 'passive' to the active state. Generally, the lower OCP in high-Ca AAMs (alkali-activated slags), when compared to OPC binders, is primarily due to the factors discussed above and must be considered when comparing OPC and AAMs. In addition, the OCP also depends on the moisture conditions at the SCI, i.e., the relative humidity to which the specimens were exposed (cf. Table 2). Nevertheless, a recent study[90] that compared chloride-induced steel corrosion in AAMs based on blast furnace slag, fly ash, and blast furnace slag/fly ash blends proposed an OCP of −400 mV versus SCE as a criterion for determining whether the

steel reinforcement in AAMs is in the active or the passive state.

5.2 | LPR measurements

The LPR method is based on the observation that the potential–current (E–i) relationship often exhibits approximate linearity for a small applied polarisation with respect to OCP ($\Delta E \approx \pm 5$–20 mV vs. OCP). Upon slight polarisation from OCP, the polarisation resistance (R_p) of the steel can be described as the ratio between the applied voltage (ΔE) and the corresponding current (Δi), R_p becoming the slope of the polarisation curve in the limit $\Delta E \to 0$ (Equation 1):

$$R_p = \left(\frac{\Delta E}{\Delta i} \right)_{\Delta E \to 0}. \tag{1}$$

The R_p values are often normalised with respect to the surface area of the metal exposed to the electrolyte and expressed in units of $k\Omega \cdot cm^2$.

LPR has often been employed to calculate the instantaneous corrosion rate (i_{corr}) of steel reinforcement embedded in concrete or mortar using the Stern-Geary equation[91] (Equation 2):

$$i_{corr} = \frac{B}{R_p} = \frac{\beta_a \beta_c}{2.3(\beta_a + \beta_c)} \cdot \frac{1}{R_p}, \tag{2}$$

where β_a and β_c are the anodic and cathodic Tafel constants (Section 5.4), respectively, and B is the proportionality constant derived from the Tafel constants.

Generally (i.e., for conventional cementitious materials as well as for AAMs), applicability of the Stern-Geary equation to calculate i_{corr} is only given if: (i) corrosion of the reinforcement is uniform, and (ii) the reinforcement is uniformly polarised. Since these conditions are almost never met in studies of steel corrosion in cementitious materials, particularly in the case of chloride-induced corrosion, the use of Equation (2) to calculate instantaneous corrosion rates in mortars and concretes is highly questionable, as has been discussed in detail by Angst and Büchler.[92] Moreover, the application of the Stern-Geary equation requires knowledge of B (or β_a and β_c). In the case of steel corrosion in OPC-based materials, the value of B has been proposed to be 26 mV for corroding steel, and 52 mV for passive steel (which stem from the empirical fitting of data from experiments conducted in solutions),[3,93] and these values have been widely adopted in subsequent studies. However, the properties of the concrete/mortar cover in AAMs (e.g., pore solution

composition and, consequently, its ionic strength and resistivity; cf. Table 4) differ from those encountered in OPC-based materials, and therefore the appropriate values of B may deviate from the values commonly used for OPC. Indeed, a study of the corrosion of steel in AAMs based on blast furnace slag/fly ash blends[25] found $B = 45$–58 mV for actively corroding steel, and $B = 13$–20 mV for passive steel, differing considerably from the above values (see Section 5.4). Similar values of $B = 55$–63 mV and $B = 15$–25 mV for the active and the passive state, respectively, of steel in various AAMs were obtained by Runci et al.[90] It is further noted that, in the context of on-site applications, it has been inferred that the LPR technique does not give reliable results for submerged concretes (that may be water saturated) or where the steel is in the passive state with restricted access to oxygen.[9]

Despite the apparent inability of the LPR method in combination with the Stern-Geary equation to quantify the corrosion rate of the steel under localised attack, the polarisation resistance (R_p) derived from LPR measurements is a useful indicator of the state (passive or actively corroding) of reinforcement steel. For OPC mortars/concretes, $R_p < 40$ kΩ·cm^2 (combined with a decrease of the OCP) has been established as a criterion for active corrosion[83,84] and found to apply also for steel in low-Ca AAMs,[63] and a significant decrease of R_p over a comparatively short time is usually an indication of the transition from the passive to the actively corroding state.

Most of the studies of steel-reinforced AAMs follow the evolution of R_p, in addition to the OCP. In the absence of aggressive species, the rebars are assumed to

be in the passive state in AAMs, as is the case for OPC. However, due to the large variability of AAM precursors and activators, the electrochemical conditions at the rebar/AAM interface may differ from OPC-based materials and between AAMs. Indeed, the variability of the R_p values measured using LPR for AAM mortars/concretes without the presence of any aggressive species (i.e., with the steel in a presumably passive state) is very high, as shown in Figure 3. The data also indicates that R_p values measured for (presumably) passive steel in high-Ca AAMs tend to be lower than those for steel in low-Ca AAMs. This behaviour has been attributed to the oxidation of sulfides in the pore solution of alkali-activated blast furnace slags (high-Ca AAMs), meaning that the R_p values measured for steel in these materials do not only represent the Fe/Fe^{2+} redox couple.[56] In fact, the polarisation resistance of steel in synthetic pore solutions simulating high-Ca AAMs has been observed to decrease with increasing HS$^-$ concentration.[56]

In the case of LPR measurements to assess the onset of steel corrosion due to chloride ingress in low-Ca AAMs, most of the studies shown in Figure 4 indicate a fairly stable R_p for a certain time after immersion in a chloride solution, followed by a sudden decrease. This R_p drop is usually interpreted as being indicative of the transition from the active to the passive state, that is, the onset of chloride-induced corrosion. However, Tittarelli et al.[45] observed a more gradual decrease of R_p during exposure to wet-dry cycles in 3.5% NaCl solution for some of their specimens. This is possibly related to the R_p at the beginning of these experiments being already very low compared to other studies of steel corrosion in low-Ca AAMs.
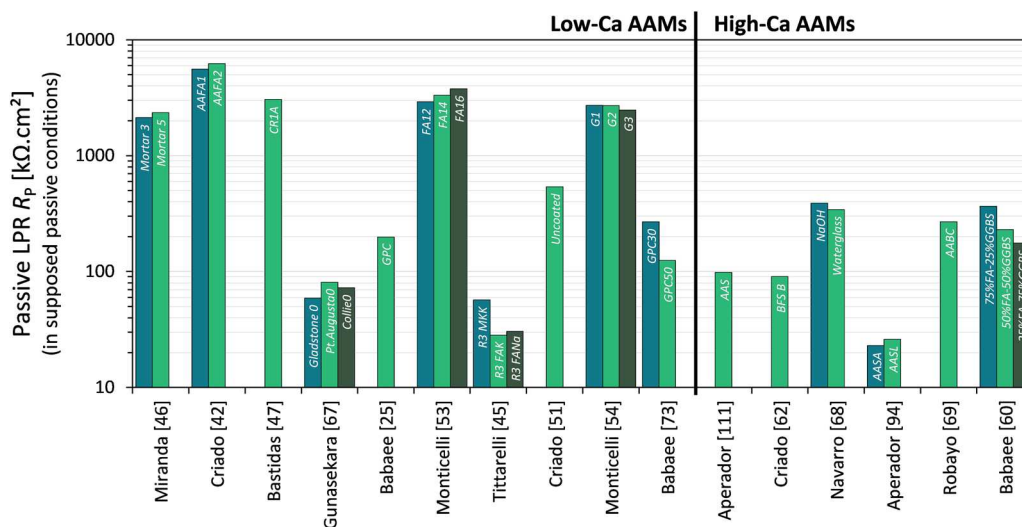

FIGURE 3 Polarisation resistances (R_p) measured using linear polarisation resistance (LPR) for steel in low-Ca and high-Ca alkali-activated materials (AAMs) before exposure to aggressive species, that is, with the steel presumably in passive condition. Sample names indicated correspond to sample names as used in the studies.
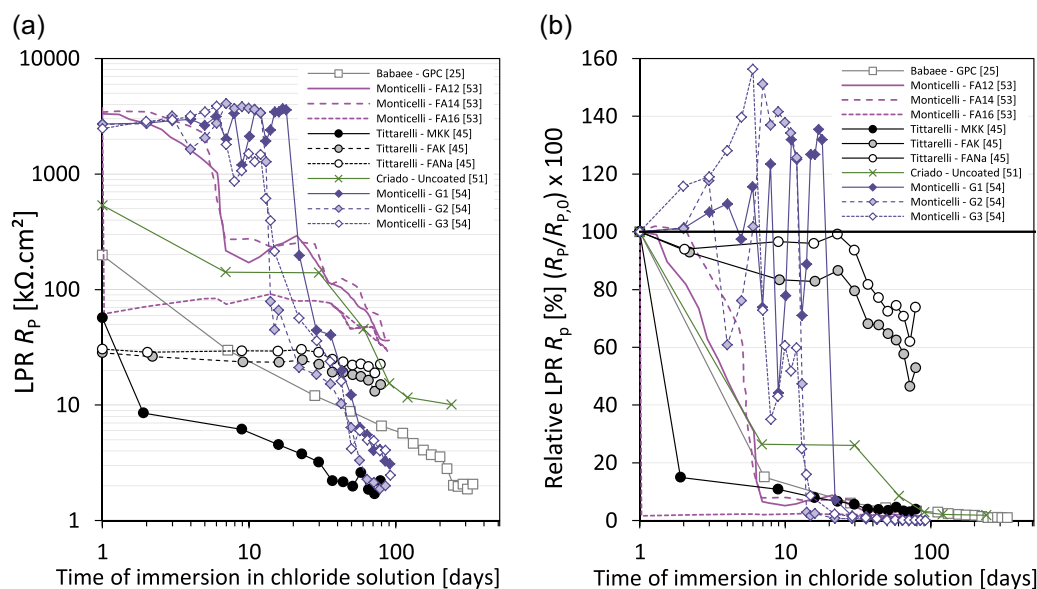
FIGURE 4 Evolution of the polarisation resistance R_p measured using linear polarisation resistance (LPR) (a: absolute values; b: relative evolution) of steel in low-Ca alkali-activated materials (AAMs) as a function of immersion time in chloride solutions. The values corresponding to the presumably passive steel (before immersion) are placed at 1 day of immersion. Sample names indicated correspond to sample names as used in the studies.

FIGURE 5 Evolution of the polarisation resistance R_p measured using linear polarisation resistance (LPR) (a: absolute values; b: relative evolution) of steel in high-Ca alkali-activated materials (AAMs) as a function of immersion time in chloride solutions. The values corresponding to the presumably passive steel (before immersion) are placed on 1 day of immersion. Sample names indicated correspond to sample names as used in the studies.
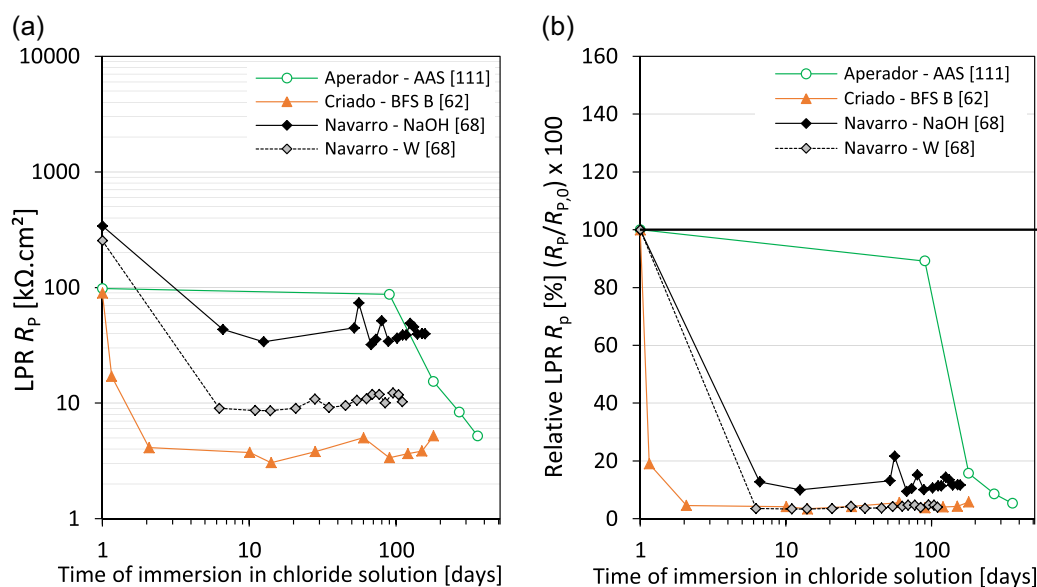
For steel reinforcement in high-Ca AAMs, most of the evaluated studies exhibited behaviour that differed from that for low-Ca AAMs: R_p decreased almost immediately after immersion in chloride solution (Figure 5). In line with this, Babaee and Castel[60] observed that in the case of steel-reinforced mortars made with alkali-activated fly ash/slag blends exposed to 3.5% NaCl solution, a clear drop in R_p during the later stages of exposure was only noticeable for samples with lower proportions of slag (< 50%). It is currently not fully established how to interpret the occurrence (or the absence) of a drop of R_p of the steel in alkali-activated blast furnace slags during

exposure to chlorides; nevertheless, it is clear that a low polarisation resistance under these conditions does not necessarily mean that corrosion initiation has occurred,[61,62] and that it can be related to the electrochemically induced oxidation of sulfides in the pore solutions of these materials.[56]

LPR has also been applied to follow the evolution of R_p of steel in AAMs exposed to atmospheres with different levels of CO_2 concentration, that is, natural and accelerated carbonation. It is usually assumed that R_p decreases when the carbonation front reaches the SCI and steel corrosion is initiated; however, this does not always occur within the timeframe of laboratory experiments (Figure 6). The reason for this behaviour can be that the carbonation front has not reached the steel surface; this is particularly likely for high-Ca AAMs, which can exhibit low carbonation coefficients.[17,68,69,94] Another possible reason is that the pH drop induced by natural carbonation (~0.04% CO_2) of AAMs is not large enough to induce depassivation and corrosion onset of the reinforcing steel[73,79]; this issue is, however, contentious and will require further studies (cf. Section 4.3). Nevertheless, the data obtained by Navarro et al.[68] for carbonation at 1% CO_2 (Figure 6) indicate that the corrosion onset of steel, induced by carbonation of AAMs, can be detected using LPR measurements.

5.3 | Measurement of concrete electrical resistivity

The electrical resistivity (ρ) of concrete and other cementitious materials is a measure of the ability of the material to inhibit the flow of electrical charge. The resistivity refers to bulk material and is often expressed in units of $\Omega \cdot cm$; it is calculated from the measured electrical resistance (R_{el} or R_Ω; in units of Ω) of a material, considering the specific test conditions (i.e., considering localised potential drops, electric field lines etc.). The measured electrical resistance of a sample relates only to the specific test conditions; nevertheless, R_{el} can be used for a comparison of materials without conversion to ρ, if all of the materials have been measured under the same conditions. Several methods have been applied to measure the electrical resistivity or the resistance of cementitious materials, for example, two external electrodes connected to opposite sides of a sample, the four-electrode Wenner probe setup, or galvanostatic pulse measurements (GPM).

The electrical resistivity of concrete has been related to the probability of corrosion or the corrosion rate, particularly in the context of the propagation phase of carbonation-induced corrosion.[4,18] However, a causal relationship between reinforcement corrosion rate in concrete structures and concrete resistivity has been critically debated and
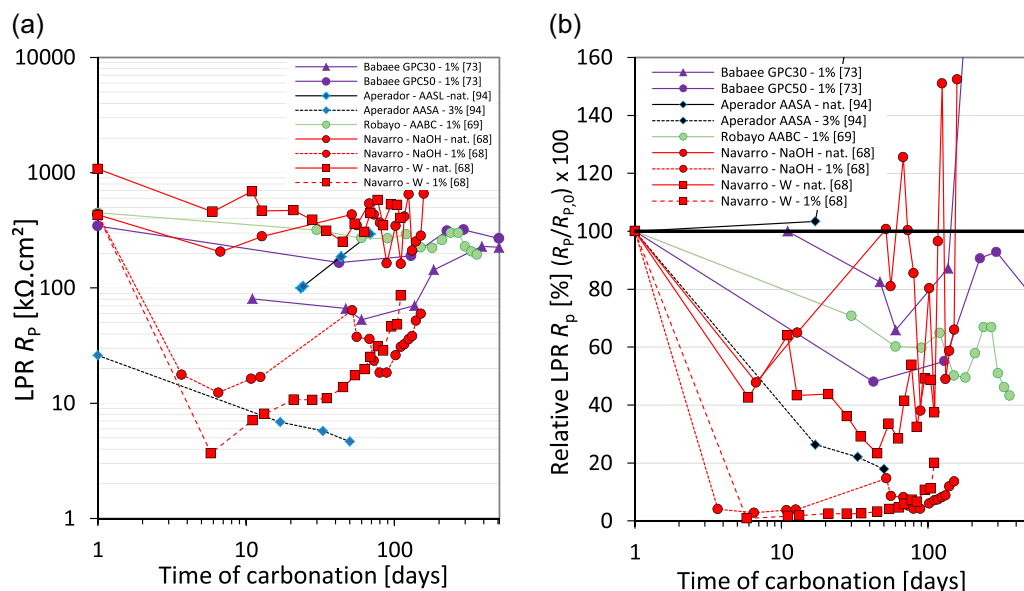

FIGURE 6 Evolution of the polarisation resistance R_p measured using linear polarisation resistance (LPR) (a: absolute values; b: relative evolution) of steel in low-Ca alkali-activated materials (AAMs) and high-Ca AAMs as a function of the time of carbonation. The values corresponding to the presumably passive steel (before exposure) are placed at 1 day of carbonation. The sample names and CO_2 concentrations (nat., natural carbonation: ~0.04%) as used in the studies are indicated in the legends. The AAMs in the study of Navarro et al.[68] were produced from SiMn slag and not from blast furnace slag; however, its S content of 2.77% (expressed as SO_3) and its negative loss on ignition (−1.25%) indicate that the SiMn slag contained a considerable amount of reduced sulfur species, similar to blast furnace slag.

essentially rejected in the recent literature.[4,95,96] Nevertheless, ρ or R_{el} remains an important parameter, as it influences the rate of both micro-cell and macro-cell corrosion,[21,22] and conveys information about the electrochemical and transport properties of cementitious materials.

The electrical resistivity of a cementitious system depends on the pore structure (porosity, pore size distribution, tortuosity) of the material, the degree of saturation of the pores, and the conductivity of the pore solution, which in turn depends on its ionic strength. Since the information about these properties is convoluted in the single parameter ρ, additional measurements (or estimates) are required to assess the individual contributions of the above characteristics. The relative importance of the individual contributions may differ strongly between conventional cementitious materials and AAMs, and between different AAMs. R_{el} has been found to be considerably lower for low-Ca AAMs than for OPC-based materials,[63,85] and this has been attributed to both a higher conductivity of the pore solution of AAMs (cf. Table 4) and a higher porosity and less tortuous pore structure of these materials.[97] In contrast, the resistivity of high-Ca AAM (alkali-activated blast furnace slag) mortars and concretes was found to be higher than that of OPC-based mortars/concretes,[52,70] despite the fact that their pore solution has a higher conductivity than the pore solution of OPC[52]; thus, the high resistance of high-Ca AAMs is mainly caused by their dense pore system, that is, their generally low porosity and fine pores.[97]

5.4 | Potentiodynamic polarisation curves

To gather kinetic and mechanistic information about the corrosion of steel, the potential of the steel can be varied (i.e., the steel is polarised) to a greater extent than is done in LPR, and the resulting current density recorded; the obtained potential–current (E–i) relationships are usually called 'anodic' polarisation curve if E is changed to more positive values than the OCP, and 'cathodic' polarisation curve if E is changed to more negative values than the OCP.[98] The procedure is destructive, that is, it changes the state of the system irreversibly. If E is plotted versus log(i) for both anodic and cathodic polarisation, the resulting plot is called the Evans diagram. The slopes of the polarisation curves in a plot of log(i) *versus* E yield the Tafel constants β_a and β_c of Equation (2); the intersection of the extrapolated anodic and cathodic polarisation curves gives an estimate of the corrosion current (i_{corr}) and the mixed potential (E_{corr}).[98]

However, the parameters calculated from polarisation curves, such as Tafel slopes, corrosion current densities etc., may be obtained under different experimental conditions and analysed using subjective decisions, thereby potentially leading to considerable scatter in the reported values.

The polarisation curves obtained for steel in the passive state in low-Ca AAMs are generally similar to those obtained for steel reinforcement in OPC-based materials.[46,54] Similar polarisation curves have also been obtained for steel in leachates obtained from a low-Ca AAM mortar and an OPC-based mortar, though the passive current densities were slightly lower for the low-Ca AAM solution, which was assigned by the authors of the study to an inhibiting effect of the dissolved silica.[53]

Chloride-induced corrosion (through admixed chlorides as well as through Cl$^-$ diffused into AAMs) induces changes in the polarisation curves, which would also be expected for conventional cementitious materials. Besides the fact that the OCP is generally shifted to lower potentials, the current densities are considerably increased at all potentials above the OCP compared to the passive state; in some cases, the corrosion currents are found to be higher by approximately two orders of magnitude than in the passive state.[25,46,47,54] Analogous behaviour was observed by Mundra et al.[55] for steel in synthetic pore solutions simulating low-Ca AAMs, where above a critical chloride concentration (dependent on the [NaOH] of the solution), the anodic polarisation curves exhibited a smaller or no passive region, and in some of these cases, the polarisation curve indicated stable or metastable pitting.

Babaee and Castel[25] applied anodic and cathodic polarisation to determine the Tafel constants, and to derive the parameter B in Equation (2), for passive steel and for steel after chloride-induced corrosion initiation in a low-Ca AAM (85% fly ash and 15% blast furnace slag in the solid binder precursors). The B value corresponding to the passive state was found to be in the range of 13–20 mV, and B for the actively corroding steel was found to be in the range of 45–58 mV. In line with these results, Robayo-Salazar et al.[69] determined $B \approx 17$–20 mV from the polarisation curves of passive steel in an AAM based on 70% natural pozzolan and 30% blast furnace slag. Potentiodynamic polarisation curves obtained Runci et al.[90] for steel reinforcement in alkali-activated blast furnace slag, alkali-activated fly ash, and alkali-activated blast furnace slag/fly ash blends also yielded $B = 15$–25 mV for passive conditions and $B = 55$–63 mV for the active state. These values deviate considerably from the values of $B = 52$, and 26 mV,[3,93] often assumed for passive and corroding steel,

respectively, in conventional concrete. However, the polarisation curves for the actively corroding steel in the AAMs were obtained after chloride-induced corrosion initiation, and the reservations discussed in Section 5.2 in the context of the LPR method apply.

The anodic polarisation curves of steel in synthetic pore solutions simulating high-Ca AAMs (i.e., containing sulfides at concentrations of 0.01 M or higher) differ considerably from the curves obtained for steel in low-Ca AAMs: an active region and a passive region cannot be clearly identified, and a peak of the current density at approx. −0.05 V versus Ag/AgCl is observed; correspondingly, the observed current densities at potentials above the OCP are considerably higher than for sulfide-free solutions (Figure 7). This behaviour can be attributed to the oxidation of HS⁻ in the solution and deposition of sulfur at the steel–solution interface, rather than the oxidation of Fe.[56]

In accordance with these observations and their interpretation, steel embedded in blast furnace slag-based high-Ca AAM mortars exhibited anodic polarisation curves with generally high current densities and a distinct current peak at ~0.1 V versus Ag/AgCl, no matter whether the specimens were stored in 1 M NaOH solution or in a solution with 1 M NaOH and 3.5% NaCl, while no corrosion products were detected in both cases.[61] Notably, the anodic polarisation curves for steel in the same AAM mortars, stored in air (50%–70% RH), were different from those for the immersed specimens, with a more positive OCP, lower current densities, and no distinct current density peak.[61] Partly deviating results were reported by Wang et al.,[59] who recorded
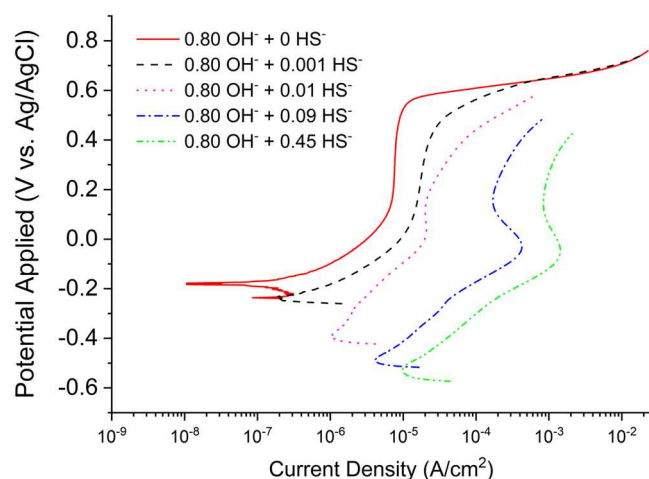
polarisation curves for steel in solutions containing only sulfur species (HS⁻, $S_2O_3^{2-}$, SO_3^{2-} and SO_4^{2-}) and in solutions containing all of these sulfur species as well as aluminate that were similar to those in the experiments described above. However, in solutions that contained the sulfur species, aluminate, and silicate (simulating the pore solution of high-Ca AAMs), they obtained polarisation curves that were similar to the polarisation curves for steel in solutions simulating the pore solutions of OPC-based materials; the authors assigned this to a passivating and inhibiting effect of the dissolved silica.

6 | OTHER ELECTROCHEMICAL TECHNIQUES

In addition to the electrochemical methods discussed in the previous sections, there are several other techniques that can, in principle, also be used to study the passivation and the corrosion of steel in AAMs. However, these techniques either have been applied only seldom to AAMs to date, so it is currently impossible to assess their specific advantages and peculiarities, or the results obtained with the technique so far do not allow to draw general conclusions, because of the complexity of the method and/or varying interpretations in different studies.

An example of the first case is the galvanostatic pulse technique.[99,100] GPM can be used to determine the polarisation resistance of reinforcing steel (R_p) as well as the resistance of the surrounding mortar or concrete (R_{el}) in a single measurement. According to Angst and Büchler,[101] conventional GPM often yields more accurate values for R_p than LPR measurements in the case of macro-cell corrosion (e.g., chloride-induced reinforcement corrosion), and the method can be even further improved by an alternative approach to evaluating the obtained data. However, to date, few studies[46,63,64] have applied GPM to study the corrosion of steel in AAMs (Table 6).

Electrochemical impedance spectroscopy (EIS)[102,103] has been applied repeatedly to study the behaviour of steel in AAMs (Table 6). In principle, this method can yield a wealth of information, though the interpretation of the obtained data depends on preliminary assumptions regarding the dominating phenomena in the system, that is, choice of a suitable equivalent electrical circuit. In the case of AAMs, several different equivalent electrical circuits have been utilised, depending on the composition/precursors of the materials and the exposure conditions.[42,43,54,61,62,70,71,94] Because of this and because of the complexity of the method, it is difficult at present to draw general conclusions as regards the applicability of EIS to study steel corrosion in AAMs as

FIGURE 7 Anodic polarisation curves of mild steel immersed in 0.80 M NaOH solutions with different sulfide concentrations (as indicated in the legend). (Reproduced from Mundra and Provis[56] published under a Creative Commons license: https://creativecommons.org/licenses/by/4.0/[CC BY 4.0]).

compared to OPC-based materials; an in-depth discussion of the related principles, advantages and problems of the method is outside the scope of the present report.

Finally, it is noted that electrochemical noise measurements hold promise for the investigation of steel corrosion in cementitious materials. One of the main reasons is that the technique does not require an externally applied current/voltage; instead, the measured current and potential fluctuations are spontaneously generated by corrosion reactions without external interference.[104,105] The coupled multi-electrode array (CMEA) is an advancement of electrochemical noise techniques. CMEA enables monitoring of spontaneously generated corrosion currents between a mesh of individual electrodes and provides both spatial and temporal information about the corrosion process. Also, with this technique, no external polarisation potential is applied. It has been rarely applied in concrete, but the results obtained so far have shown that the detection of anodic and cathodic sites as well as the assessment of local corrosion rates over time, is possible in conventional cementitious materials,[106–109] and first attempts to monitor steel corrosion processes in AAMs by means of CMEA have been made.[110]

7 | SUMMARY AND CONCLUDING REMARKS

A considerable body of data is now available with regard to the corrosion of steel reinforcement in AAMs. These include testing and analysis of steel in several different surface conditions; however, a systematic study investigating the impact of different surface conditions on the behaviour of the steel and the outcomes of electrochemical tests has not yet been conducted. Likewise, systematic studies of the effect of the moisture conditions (degree of water saturation) at SCI on the corrosion of steel in AAMs are not available. Nevertheless, the work done so far has yielded some important insights into behaviour of steel in AAMs within a wide compositional range. The present analysis of the available data has demonstrated that important differences exist between AAMs and conventional (OPC-based) cementitious materials, and between different classes of AAMs (low-Ca and high-Ca), mainly caused by differing pore solution compositions, and that these differences influence the outcomes and the accurate interpretation of electrochemical measurements concerning the corrosion of steel reinforcement in AAMs.

An important characteristic of the pore solutions of high-Ca AAMs (alkali-activated blast furnace slags) is that high concentrations of reduced sulfur species

(sulfide, polysulfides) are usually present. This creates redox couples in addition to the Fe/Fe^{2+} couple, yielding distinct polarisation curves, and generally leading to much lower OCPs and often lower measured (apparent) polarisation resistances of embedded steel than those observed in low-Ca AAMs and OPC-based materials. If the specific characteristics of the pore solution of high-Ca AAMs are not taken into account and recommendations for conventional cementitious materials (e.g., RILEM TC 154-EMC and ASTM C876) are applied without modifications, this may lead to erroneous interpretations and 'detection' of active steel corrosion. The same arguments apply to the application of electrochemical methods to conventional OPC-based slag-containing cements, such as CEM III/B.

On the contrary, OCP, LPR and anodic polarisation of low-Ca AAMs yield results that can be interpreted in a way very similar to OPC-based materials. It is important to note, however, that there are indications that steel in low-Ca AAMs requires much more time (up to several weeks) for the establishment of a stable passive layer, which needs to be accounted for in studies that presume a passive state before subsequent measurement. Non-compliance with the latter requirement as well as the inadequate introduction of aggressive species into the material, may explain some of the discrepancies found in the literature on the topic.

For both classes of AAMs, studies of carbonation-induced steel corrosion present difficulties different from those for OPC-based materials. There are indications that corrosion initiation does not occur under testing conditions that approximate natural conditions, while it is unclear at present how accelerated carbonation should be performed to obtain results that are representative of real-world conditions. In addition, high-Ca AAMs can possess pore structure characteristics that can make it impossible to initiate corrosion within the timeframe of normal laboratory experiments under at least reasonably representative conditions.

It is important to restate that, generally, LPR can yield accurate quantitative data only when steel corrosion is non-localised, that is, strictly, it is not applicable to chloride-induced corrosion. If LPR is applied anyway to measure R_p and calculate i_{corr} via the Stern-Geary equation, it must be considered that the required proportionality constants for steel in AAMs have been determined to be significantly different from those for OPC-based materials. As only little data are available in this regard, additional work is required to confirm or adjust the values that have been proposed.

Measurements of the resistivity (or resistance) of AAMs, which is particularly important in the context of macro-cell corrosion, show that the resistivity of low-Ca

AAMs is generally much lower than that of OPC-based materials, due to a higher conductivity of their pore solution and a coarser pore structure. For high-Ca AAMs, a higher resistivity than for OPC-based materials was found, attributable to their fine pore structure. However, data regarding how shrinkage and associated cracking will influence this characteristic of the latter materials are scarce.

Most of the studies evaluated in the present analysis report measurements of OCP, LPR, polarisation curves, and/or EIS to obtain information about the passivation and corrosion of steel in AAMs. While these techniques are highly adequate to study the pertinent phenomena, each of them has certain limitations, as discussed in the present report. It thus appears that the application of alternative electrochemical techniques, such as GPM, electrochemical noise measurements/coupled multi-electrode array, may lead to additional insights. In addition, it seems worthwhile to shift the focus of future studies of steel corrosion in AAMs more towards the effects of the conditions at the SCI, in line with current trends in the field of steel corrosion in conventional concretes.

DATA AVAILABILITY STATEMENT
Data sharing is not applicable to this article as no new data were created in this study.

ORCID
Shishir Mundra http://orcid.org/0000-0001-6559-8814
Gabriel Samson http://orcid.org/0000-0002-3472-8089
Giulia Masi http://orcid.org/0000-0001-5204-2059
Rebecca Achenbach http://orcid.org/0000-0001-5367-8075
David M. Bastidas http://orcid.org/0000-0002-8720-7500
Susan A. Bernal http://orcid.org/0000-0002-9647-3106
Maria C. Bignozzi http://orcid.org/0000-0002-1939-5909
Maria Criado http://orcid.org/0000-0002-1027-6233
Martin Cyr http://orcid.org/0000-0002-5012-9131
Nina Gartner http://orcid.org/0000-0002-3770-6555
Stefanie von Greve-Dierfeld http://orcid.org/0000-0002-9556-2027
Andraž Legat http://orcid.org/0000-0001-7775-1919
Ali Nikoonasab http://orcid.org/0000-0002-0561-8980
John L. Provis http://orcid.org/0000-0003-3372-8922
Michael Raupach http://orcid.org/0000-0003-0688-3839
Gregor J. G. Gluth http://orcid.org/0000-0002-8951-7393

REFERENCES
[1] L. Bertolini, B. Elsener, P. Pedeferri, E. Redaelli, R. B. Polder, Corrosion of Steel in Concrete: Prevention, Diagnosis, Repair, 2nd ed., Wiley-VCH, Weinheim **2013**.

[2] U. M. Angst, *Mater. Struct.* **2018**, *51*, 4.

[3] C. Andrade, J. A. González, *Mater. Corros.* **1978**, *29*, 515.

[4] M. Stefanoni, U. Angst, B. Elsener, *Cem. Concr. Res.* **2018**, *103*, 35.

[5] C. Andrade, M. C. Alonso, J. A. González, *Corros. Rates Steel Concr.*, ASTM, Philadelphia **1990**, pp. 29.

[6] M. Alexander, M. Thomas, *Cem. Concr. Res.* **2015**, *78*, 155.

[7] U. M. Angst, M. R. Geiker, M. C. Alonso, R. Polder, O. B. Isgor, B. Elsener, H. Wong, A. Michel, K. Hornbostel, C. Gehlen, R. François, M. Sanchez, M. Criado, H. Sørensen, C. Hansson, R. Pillai, S. Mundra, J. Gulikers, M. Raupach, J. Pacheco, A. Sagüés, *Mater. Struct.* **2019**, *52*, 88.

[8] B. Elsener, C. Andrade, J. Gulikers, R. Polder, M. Raupach, *Mater. Struct.* **2003**, *36*, 461.

[9] C. Andrade, C. Alonso, *Mater. Struct.* **2004**, *37*, 623.

[10] K. L. Scrivener, V. M. John, E. M. Gartner, *Eco-efficient Cements: Potential, Economically Viable Solutions for a Low-CO_2, Cement-based Materials Industry*, United Nations Environment Programme, Paris. **2016**.

[11] J. L. Provis, *Mater. Struct.* **2014**, *47*, 11.

[12] J. L. Provis, J. S. J. van Deventer, *Alkali Activated Materials: State-of-the-art Report, RILEM TC 224-AAM*, Springer, Dordrecht **2014**.

[13] J. L. Provis, S. A. Bernal, *Annu. Rev. Mater. Res.* **2014**, *44*, 299.

[14] S. Mundra, D. P. Prentice, S. A. Bernal, J. L. Provis, *Cem. Concr. Res.* **2020**, *130*, 106011.

[15] S. A. Bernal, R. San Nicolas, J. L. Provis, R. Mejía de Gutiérrez, J. S. J. van Deventer, *Mater. Struct.* **2014**, *47*, 693.

[16] G. J. G. Gluth, K. Arbi, S. A. Bernal, D. Bondar, A. Castel, S. Chithiraputhiran, A. Dehghan, K. Dombrowski-Daube, A. Dubey, V. Ducman, K. Peterson, P. Pipilikaki, S. L. A. Valcke, G. Ye, Y. Zuo, J. L. Provis, *Mater. Struct.* **2020**, *53*, 21.

[17] G. J. G. Gluth, X. Ke, A. Vollpracht, L. Weiler, S. A. Bernal, M. Cyr, K. Dombrowski-Daube, D. A. Geddes, C. Grengg, C. Le Galliard, M. Nedeljkovic, J. L. Provis, L. Valentini, B. Walkley, *Mater. Struct.* **2022**, *55*, 225.

[18] C. Alonso, C. Andrade, J. A. González, *Cem. Concr. Res.* **1988**, *18*, 687.

[19] G. K. Glass, C. L. Page, N. R. Short, *Corros. Sci.* **1991**, *32*, 1283.

[20] L. Tang, J. M. Frederiksen, U. M. Angst, R. Polder, M. C. Alonso, B. Elsener, D. Hooton, J. Pacheco, *RILEM Tech. Lett.* **2018**, *3*, 25.

[21] C. Andrade, I. R. Maribona, S. Feliu, J. A. González, S. Feliu, Jr., *Corros. Sci.* **1992**, *33*, 237.

[22] M. Raupach, *Constr. Build. Mater.* **1996**, *10*, 329.

[23] U. M. Angst, M. R. Geiker, A. Michel, C. Gehlen, H. Wong, O. B. Isgor, B. Elsener, C. M. Hansson, R. François, K. Hornbostel, R. Polder, M. C. Alonso, M. Sanchez, M. J. Correia, M. Criado, A. Sagüés, N. Buenfeld, *Mater. Struct.* **2017**, *50*, 143.

[24] B. Elsener, *Cem. Concr. Compos.* **2002**, *24*, 65.

[25] M. Babaee, A. Castel, *Cem. Concr. Res.* **2016**, *88*, 96.

[26] C. Boschmann Käthler, U. M. Angst, A. M. Aguilar, B. Elsener, *Corros. Sci.* **2019**, *157*, 331.

[27] X. Zhang, Y. Zhao, S. A. Bernal, *Mater. Struct.* **2021**, *54*, 55.

[28] U. Angst, B. Elsener, C. K. Larsen, Ø. Vennesland, *Cem. Concr. Res.* **2009**, *39*, 1122.

[29] ASTM C876-22b. *Standard Test Method for Corrosion Potentials of Uncoated Reinforcing Steel in Concrete*. ASTM International, **2022**.

[30] J. C. Kliethermes, *Repair of Spalling Bridge Decks: Bridge Design, Construction and Repair*, Highway Research Board National Research Council, Washington, DC **1972**, pp. 83–92.

[31] J. R. van Daveer, *ACI J.* **1975**, *72*, 697.

[32] R. R. Lloyd, J. L. Provis, J. S. J. van Deventer, *Cem. Concr. Res.* **2010**, *40*, 1386.

[33] P. Duxson, G. C. Lukey, F. Separovic, J. S. J. van Deventer, *Ind. Eng. Chem. Res.* **2005**, *44*, 832.

[34] F. Puertas, A. Fernández-Jiménez, M. T. Blanco-Varela, *Cem. Concr. Res.* **2004**, *34*, 139.

[35] S. Song, H. M. Jennings, *Cem. Concr. Res.* **1999**, *29*, 159.

[36] A. Gruskovnjak, B. Lothenbach, L. Holzer, R. Figi, F. Winnefeld, *Adv. Cem. Res.* **2006**, *18*, 119.

[37] R. J. Myers, S. A. Bernal, J. L. Provis, *Cem. Concr. Res.* **2014**, *66*, 27.

[38] M. Chaouche, X. X. Gao, M. Cyr, M. Cotte, L. Frouin, *J. Am. Ceram. Soc.* **2017**, *100*, 1707.

[39] A. Vollpracht, B. Lothenbach, R. Snellings, J. Haufe, *Mater. Struct.* **2016**, *49*, 3341.

[40] Y. Zuo, M. Nedeljković, G. Ye, *Cem. Concr. Res.* **2019**, *115*, 230.

[41] F. P. Glasser, K. Luke, M. J. Angus, *Cem. Concr. Res.* **1988**, *18*, 165.

[42] M. Criado, D. M. Bastidas, S. Fajardo, A. Fernández-Jiménez, J. M. Bastidas, *Cem. Concr. Compos.* **2011**, *33*, 644.

[43] C. Monticelli, M. Criado, S. Fajardo, J. M. Bastidas, M. Abbottoni, A. Balbo, *Cem. Concr. Res.* **2014**, *55*, 49.

[44] J. Shi, J. Ming, M. Wu, *Cem. Concr. Compos.* **2020**, *108*, 103532.

[45] F. Tittarelli, A. Mobili, C. Giosuè, A. Belli, T. Bellezze, *Corros. Sci.* **2018**, *134*, 64.

[46] J. M. Miranda, A. Fernández-Jiménez, J. A. González, A. Palomo, *Cem. Concr. Res.* **2005**, *35*, 1210.

[47] D. M. Bastidas, A. Fernández-Jiménez, A. Palomo, J. A. González, *Corros. Sci.* **2008**, *50*, 1058.

[48] M. Criado, C. Monticelli, S. Fajardo, D. Gelli, V. Grassi, J. M. Bastidas, *Constr. Build. Mater.* **2012**, *35*, 30.

[49] K. Kupwade-Patil, E. N. Allouche, *J. Mater. Civ. Eng.* **2013**, *25*, 1465.

[50] M. Sufian Badar, K. Kupwade-Patil, S. A. Bernal, J. L. Provis, E. N. Allouche, *Constr. Build. Mater.* **2014**, *61*, 79.

[51] M. Criado, I. Sobrados, J. M. Bastidas, J. Sanz, *Prog. Org. Coat.* **2016**, *99*, 11.

[52] Q. Ma, S. V. Nanukuttan, P. A. M. Basheer, Y. Bai, C. Yang, *Mater. Struct.* **2016**, *49*, 3663.

[53] C. Monticelli, M. E. Natali, A. Balbo, C. Chiavari, F. Zanotto, S. Manzi, M. C. Bignozzi, *Cem. Concr. Res.* **2016**, *80*, 60.

[54] C. Monticelli, M. E. Natali, A. Balbo, C. Chiavari, F. Zanotto, S. Manzi, M. C. Bignozzi, *Cem. Concr. Res.* **2016**, *87*, 53.

[55] S. Mundra, M. Criado, S. A. Bernal, J. L. Provis, *Cem. Concr. Res.* **2017**, *100*, 385.

[56] S. Mundra, J. L. Provis, *J. Mater. Sci.* **2021**, *56*, 14783.

[57] J. Shi, J. Ming, W. Sun, *Constr. Build. Mater.* **2017**, *155*, 992.

[58] C. Tennakoon, A. Shayan, J. G. Sanjayan, A. Xu, *Mater. Des.* **2017**, *116*, 287.

[59] W. Wang, H. Chen, X. Li, Z. Zhu, *Constr. Build. Mater.* **2017**, *143*, 289.

[60] M. Babaee, A. Castel, *Cem. Concr. Res.* **2018**, *111*, 56.

[61] M. Criado, S. A. Bernal, P. Garcia-Triñanes, J. L. Provis, *J. Mater. Sci.* **2018**, *53*, 5016.

[62] M. Criado, J. L. Provis, *Front. Mater.* **2018**, *5*, 34.

[63] G. J. G. Gluth, G. Ebell, P. Hlaváček, J. Mietz, *Mater. Corros.* **2020**, *71*, 749.

[64] G. J. G. Gluth, P. Hlaváček, S. Reinemann, G. Ebell, J. Mietz, *MATEC Web Conf.* **2018**, *199*, 02025.

[65] J. Shi, J. Ming, W. Sun, *Corros. Sci.* **2018**, *133*, 288.

[66] X. Yu, L. Jiang, J. Xu, *J. Mater. Civ. Eng.* **2018**, *30*, 04018146.

[67] C. Gunasekara, D. Law, S. Bhuiyan, S. Setunge, L. Ward, *Constr. Build. Mater.* **2019**, *200*, 502.

[68] R. Navarro, E. G. Alcocel, I. Sánchez, P. Garcés, E. Zornoza, *Constr. Build. Mater.* **2020**, *230*, 116917.

[69] R. A. Robayo-Salazar, A. M. Aguirre-Guerrero, R. Mejía de Gutiérrez, *Constr. Build. Mater.* **2020**, *232*, 117189.

[70] J. Shi, M. Wu, J. Ming, *Corros. Sci.* **2021**, *179*, 109175.

[71] N. Gartner, M. Hren, T. Kosec, A. Legat, *Materials* **2021**, *14*, 7366.

[72] R. San Nicolas, J. L. Provis, *Front. Mater.* **2015**, *2*, 70.

[73] M. Babaee, M. S. H. Khan, A. Castel, *Cem. Concr. Compos.* **2018**, *85*, 32.

[74] NT BUILD 443. *Concrete, Hardened: Accelerated Chloride Penetration, Nordtest*, **1995**.

[75] EN 206. *Concrete - Specification, Performance, Production and Conformity, CEN,* **2013**.

[76] D. Trejo, R. G. Pillai, *ACI Mater. J.* **2003**, *100*, 519.

[77] D. Trejo, R. G. Pillai, *ACI Mater. J.* **2004**, *101*, 57.

[78] R. Hay, C. P. Ostertag, *Cem. Concr. Compos.* **2020**, *110*, 103573.

[79] S. A. Bernal, J. L. Provis, D. G. Brice, A. Kilcullen, P. Duxson, J. S. J. van Deventer, *Cem. Concr. Res.* **2012**, *42*, 1317.

[80] M. Stefanoni, U. Angst, B. Elsener, *Cem. Concr. Compos.* **2020**, *113*, 103717.

[81] U. Angst, F. Moro, M. Geiker, S. Kessler, H. Beushausen, C. Andrade, J. Lahdensivu, A. Köliö, K. i Imamoto, S. Von Greve-Dierfeld, M. Serdar, *RILEM Tech. Lett.* **2020**, *5*, 85.

[82] M. Pourbaix, *Corros. Sci.* **1965**, *5*, 677.

[83] U. M. Angst, B. Elsener, C. K. Larsen, Ø. Vennesland, *Corros. Sci.* **2011**, *53*, 1451.

[84] U. M. Angst, C. Boschmann, M. Wagner, B. Elsener, *J. Visual. Exp.* **2017**.

[85] S. Mundra, S. A. Bernal, M. Criado, P. Hlaváček, G. Ebell, S. Reinemann, G. J. G. Gluth, J. L. Provis, *RILEM Tech. Lett.* **2017**, *2*, 33.

[86] M. Holloway, J. M. Sykes, *Corros. Sci.* **2005**, *47*, 3097.

[87] M. J. Angus, F. P. Glasser, *Mater. Res. Soc. Symp. Proc.* **2005**, *50*, 547.

[88] V. Garcia, R. François, M. Carcasses, P. Gegout, *Mater. Struct.* **2014**, *47*, 1483.

[89] A. Scott, M. G. Alexander, *Cem. Concr. Res.* **2016**, *89*, 45.

[90] A. Runci, J. L. Provis, M. Serdar, *Corros. Sci.* **2023**, *210*, 110849.

[91] M. Stern, A. L. Geary, *J. Electrochem. Soc.* **1957**, *104*, 56.

[92] U. Angst, M. Büchler, *Mater. Corros.* **2015**, *66*, 1017.

[93] C. Andrade, C. Alonso, *Constr. Build. Mater.* **1996**, *10*, 315.

[94] W. Aperador Chaparro, R. Mejía de Gutiérrez, D. M. Bastidas, *Corros. Sci.* **2009**, *51*, 2027.

[95] K. Hornbostel, C. K. Larsen, M. R. Geiker, *Cem. Concr. Compos.* **2013**, *39*, 60.

[96] M. Stefanoni, U. M. Angst, B. Elsener, *Sci. Rep.* **2018**, *8*, 7407.

[97] J. L. Provis, R. J. Myers, C. E. White, V. Rose, J. S. J. van Deventer, *Cem. Concr. Res.* **2012**, *42*, 855.

[98] A. J. Bard, L. R. Faulkner, *Electrochemical Methods: Fundamentals and Applications*, 2nd ed., Wiley, New York **2001**.

[99] C. J. Newton, J. M. Sykes, *Corros. Sci.* **1988**, *28*, 1051.

[100] B. Elsener, H. Wojtas, H. Böhni, *Corrosion and Corrosion Protection of Steel in Concrete*, 1, Sheffield Academic Press, Sheffield **1994**, p. 236.

[101] U. Angst, M. Büchler, *Mater. Corros.* **2020**, *71*, 808.

[102] D. D. Macdonald, *Electrochim. Acta* **2006**, *51*, 1376.

[103] D. Ende, K.-M. Mangold, *Chem. Unserer Zeit* **1993**, *27*, 134.

[104] K. Videm, *Mater. Sci. Forum* **1998**, *289–292*, 3.

[105] A. Legat, M. Leban, Ž. Bajt, *Electrochim. Acta* **2004**, *49*, 2741.

[106] A. Legat, *Electrochim. Acta* **2007**, *52*, 7590.

[107] A. Česen, T. Kosec, A. Legat, *Corros. Sci.* **2013**, *75*, 47.

[108] M. Hren, T. Kosec, A. Legat, *Constr. Build. Mater.* **2019**, *221*, 604.

[109] N. Gartner, T. Kosec, A. Legat, *Materials* **2020**, *13*, 407.

[110] N. Gartner, M. Hren, T. Kosec, A. Legat, *Presented at 74th RILEM Annual Week & 40th Cement and Concrete Science Conference*, Sheffield, UK, **2020**, 155.

[111] W. Aperador Chaparro, J. Hernando Bautista Ruiz, R. D. J. Torres, *Mater. Res.* **2012**, *15*, 57.